PROCEEDINGS OF SCIENCE

Observational Tensions in Kinetically Coupled Quintessence

Elsa M. Teixeira

School of Mathematics and Statistics, University of Sheffield, Hounsfield Road, Sheffield S3 7RH, United Kingdom

E-mail: emcteixeira1@sheffield.ac.uk

We study and analyse a particular example of an interacting dark energy model with explicit dependence on the kinetic term of the scalar field, simply characterised by a power-law coupling function acting on dark matter only. The emergence of novel early-time scaling solutions in such scenarios enhances their theoretical interest by alleviating the coincidence problem, before the current period of accelerated expansion. A thorough analysis of the background evolution and linear scalar perturbations of the model pinpoints the signatures left by the coupling in the dark sector on the observables, namely the cosmic microwave background, lensing potential auto-correlation, and matter power spectra. A primary parameter estimation analysis, which incorporates data from cosmic microwave background temperature and polarisation, lensing, baryonic acoustic oscillations, and supernovae distance *moduli*, reveals a non-vanishing prediction for the coupling strength between the dark sectors, encoded in the power-law parameter α, bounded to the order of 10^{-4}. While a model selection analysis using simple statistical indicators does not point to a preferred setting, a full Bayesian evidence study favours the standard ΛCDM model.

Corfu Summer Institute 2022 "School and Workshops on Elementary Particle Physics and Gravity", 28 August - 1 October, 2022
Corfu, Greece

PoS(CORFU2022)217

1. Introduction

Recent advances in observational methods and numerical techniques have enabled cosmologists to constrain the parameters of the standard cosmological model, known as Lambda-Cold-Dark-Matter [1], with outstanding accuracy. This model has its gravitational roots in Einstein's General Relativity, which remains the most successful theory of gravitation to date. It has withstood numerous tests while successfully describing the Universe's behaviour at both small and large scales. However, to properly account for the Universe's history, modern cosmology requires the inclusion of two enigmatic components: dark matter (DM) and dark energy (DE). Despite constituting a striking share of 95% of the Universe's total matter content, the nature and properties of both these "dark" components is still not fully understood. DM is widely considered as a pressureless and weakly interacting matter component that is a crucial ingredient in the mechanism of structure formation in the Universe and to the dynamics and motion of galaxies. On the other hand, DE was introduced as the driving source for the late-time acceleration of the Universe, discovered in 1998 [2, 3] and which could not be accounted for by conventional particle physics theory. In the past 25 years a growing number of independent probing methods keeps endorsing the need for a more concrete understanding of the nature of DE, detectable through distinguishable signatures on cosmological observables. This has been made possible by the rapid progress in precision data collection, leading to the urgency of resolving the mystery of these dark components.

In the standard cosmological model, ΛCDM, dark energy is simply portrayed as a cosmological constant Λ, akin to some characteristic vacuum energy of the Universe, which remains constant throughout its expansion. Albeit initially yielding great consistency confirmation in favour of ΛCDM, the recent advent of observational precision and techniques has uncovered unforeseen problems exposed as tensions between various probes, introducing a new crisis in the standard model of cosmology [4–8]. These tensions arise from discrepancies between observations of the early and late stages of the Universe, such as those of the Planck cosmic microwave background (CMB) data and varied distance-ladder surveys, respectively. Arguably the most prominent issue, the Hubble tension [9–11] arises from measurements of the current cosmic expansion rate in the Universe, H_0, best illustrated by the discrepancy between the value inferred from the Planck satellite [12] ($H_0 = 67.4 \pm 0.5$ km s^{-1} Mpc^{-1}) and the distance-ladder measurements of type Ia supernovae data calibrated with Cepheid stars by the SH0ES collaboration [13] ($H_0 = 73.04 \pm 1.04$ km s^{-1} Mpc^{-1}). Although part of these discrepancies could be attributed to data errors and systematics, the statistical significance of roughly a 5σ tension suggests flaws in the standard model itself, with many extensions being proposed in the literature as an attempt to ease this problem. Exploring alternative models may reveal new insights into the enigmatic nature of the dark sector, the physics of the early Universe, or even the fundamental assumptions of ΛCDM [14].

In Ref. [15] we have studied a particular extension in which DE is portrayed by a canonical scalar field (*quintessence*), coupled to DM through an interaction term in action, as proposed in Ref. [16]. We performed a thorough numerical analysis of the dynamics of the model under consideration, both at the background and linear perturbative levels. As in previous coupled quintessence studies [17–21], we also derived constraints for the cosmological and model-specific parameters according to different data-sets from which we found that although the cosmic tensions persist in the *best-fit* realisation of the model, there is a non-zero prediction for deviations from

the standard model encoded by the coupling parameter. A preliminary analysis of the statistical preference of the Kinetic model over ΛCDM through the effective χ^2 and the Deviation Information Criteria revealed no statistical preference for any of the models. Here we show that the full Bayesian analysis actually indicates significant preference for the standard model, as the Bayes factor properly accounts for the increased complexity introduced when adding more parameters.

2. Theoretical Motivation

Let's begin by considering a phenomenological theory in the Einstein frame, where dark energy in the form of a dynamical quintessence field, denoted as ϕ, is minimally coupled to gravity. The DE source interacts with a dark matter component as expressed in the following action [16]:

$$\mathcal{S} = \int \mathrm{d}^4x\sqrt{-g}\left[\frac{\mathrm{M}_{\mathrm{Pl}}^2}{2}R + X - V(\phi) + f(X)\tilde{\mathcal{L}}_c(\zeta, g_{\mu\nu}) + \mathcal{L}_{\mathrm{SM}}(\psi_i, g_{\mu\nu})\right] . \tag{1}$$

Here, g represents the determinant of the metric tensor $g_{\mu\nu}$, R is the curvature scalar, and $\mathrm{M}_{\mathrm{Pl}}^2 = (8\pi G)^{-1}$ corresponds to the Planck mass in units where $c = 1$, with G being the Newtonian constant. The second and third terms in the action represent the Lagrangian of the scalar field, where $X = -g^{\mu\nu}\partial_\mu\phi\partial_\nu\phi/2$ represents the kinetic term of ϕ, and $V(\phi)$ is the self-interacting potential of the scalar field. The standard model is further extended by the introduction of a purely kinetic function $f(X)$ that multiplies the Lagrangian of cold dark matter [16], $\mathcal{L}_c \equiv f(X)\tilde{\mathcal{L}}_c$, leading to a coupling between ϕ and the dark matter fields ζ. In particular, we focus on the simplest power-law kinetic interaction, as motivated in Ref. [16], described by the function:

$$f(X) = \left(\frac{\mathrm{M}_{\mathrm{Pl}}^{-4}X}{\alpha}\right)^{\alpha} \quad \Longrightarrow \quad Q = -\rho_c\frac{\alpha}{X}\left(\Box\phi + \frac{\partial^\mu\phi\partial_\nu\phi\nabla_\mu\partial^\nu\phi}{X} + \partial^\mu\phi\frac{\partial_\mu\rho_c}{\rho_c}\right) , \tag{2}$$

where α is a dimensionless constant governing the strength of the coupling Q in the dark sector and ρ_c represents the energy density of the cold dark matter. We assume a simple exponential potential for the quintessence field:

$$V(\phi) = V_0\exp\left(-\frac{\lambda\phi}{\mathrm{M}_{\mathrm{Pl}}}\right) , \tag{3}$$

where V_0 represents the energy scale of the potential, and λ characterises its steepness. These choices for the coupling function and potential are motivated by the desire to have a scaling regime [16] at early times, followed by an accelerated expansion driven by the scalar field. The exponential potential drives the system out of the scaling solution and towards the late-time attractor.

It should be noted that the action described by Eq. (1) is mathematically equivalent to a scalar-tensor theory in the Einstein frame with a conformal coupling in the DM action $\mathcal{S}_c\left[\tilde{g}_{\mu\nu}(X), \zeta\right]$. The coupling arises *via* the conformal function $C(X) = f^2(X)$ in the metric transformation $\tilde{g}_{\mu\nu} = C(X)g_{\mu\nu}$, with a fundamentally different physical interpretation.

3. Numerical Analysis

3.1 Background Dynamics

We assume cosmological dynamics in a flat Friedmann-Lemaître-Robertson-Walker (FLRW) background, expressed by the scale factor of the Universe $a(\tau)$ in conformal time τ:

$$\mathrm{d}s^2 = a(\tau)^2 \left(-\mathrm{d}\tau^2 + \delta_{ij}\mathrm{d}x^i\mathrm{d}x^j\right) . \tag{4}$$

The equations governing the background evolution are obtained through variation of the action according to the metric and the scalar degree of freedom, namely the modified Friedmann equation and conservation relations:

$$\begin{aligned}
3\mathrm{M}_{\mathrm{Pl}}^2\mathcal{H}^2 &= a^2(\rho_c + \rho_b + \rho_r + \rho_\phi) , && (5)\\
\phi'' + 2\mathcal{H}\phi' + a^2 V_{,\phi} &= a^2 Q , && (6)\\
\rho'_\phi + 3\mathcal{H}(1 + w_\phi)\rho_\phi &= Q\phi' , && (7)\\
\rho'_c + 3\mathcal{H}\rho_c &= -Q\phi' , && (8)\\
\rho'_b + 3\mathcal{H}\rho_b &= 0 , && (9)\\
\rho'_r + 4\mathcal{H}\rho_r &= 0 , && (10)
\end{aligned}$$

respectively, and with $' \equiv \mathrm{d}/\mathrm{d}\tau$ and $\mathcal{H} = \frac{a'}{a}$ is the conformal Hubble rate. The coupling Q given in Eq. (2) becomes:

$$Q = 2\alpha\rho_c \frac{3\mathcal{H}\phi' + a^2 V_{,\phi}}{2\alpha a^2\rho_c + (1 + 2\alpha)\,\phi'^2} . \tag{11}$$

Eqs. (8) and (7) imply that when $Q\phi' > 0$, energy is transferred from the cold dark matter source to the scalar field, and *vice versa* when $Q\phi' < 0$. For numerical purposes, the value of V_0 in the potential, is used in a shooting method. As a result $\{\lambda, \alpha\}$ are the model's free parameters. The viable parameter space has been studied in Ref. [15] according to dynamical and stability conditions, along with motivation for the particular initial conditions for the scalar field used in the simulations. We resort to numerical simulations using a modified version of the Einstein-Boltzmann solver `CLASS` [22–24] to study the predictions of the model over the expansion history for different $\{\lambda, \alpha\}$ combinations, using standard *Planck* 2018 [12] reference values for the cosmological parameters.

In the left panel of Fig. 1, we present the evolution of the relative energy densities $\Omega_i = \rho_i a^2/(3\mathrm{M}_{\mathrm{Pl}}^2\mathcal{H}^2)$ for each species with respect to redshift $(1 + z)$. As expected, the introduction of the coupling leads to the emergence of an early scaling regime during the radiation-dominated epoch, where the energy density of the scalar field is proportional to that of dark matter, approximately following the relation $\rho_c/\rho_\phi = 1/\alpha$, as shown in the upper right panel of Fig. 1. Eventually, the field exits this scaling regime and transitions towards the future attractor solution, causing its energy density to continuously dilute as $\rho_\phi \propto a^{-\lambda^2}$. For the values considered, the coupling strength $Q\phi'/\rho_c$ remains positive at all redshifts, implying a transfer of energy from the dark matter fluid to the scalar field. It should be noted that by fixing the present-day values of fluid densities, the energy density of cold dark matter is relatively higher at earlier times due to its contribution in supplying energy to the scalar field at later times. This effect becomes more pronounced for larger values of α. As the DM energy density decreases over time, the additional energy transferred to the scalar field

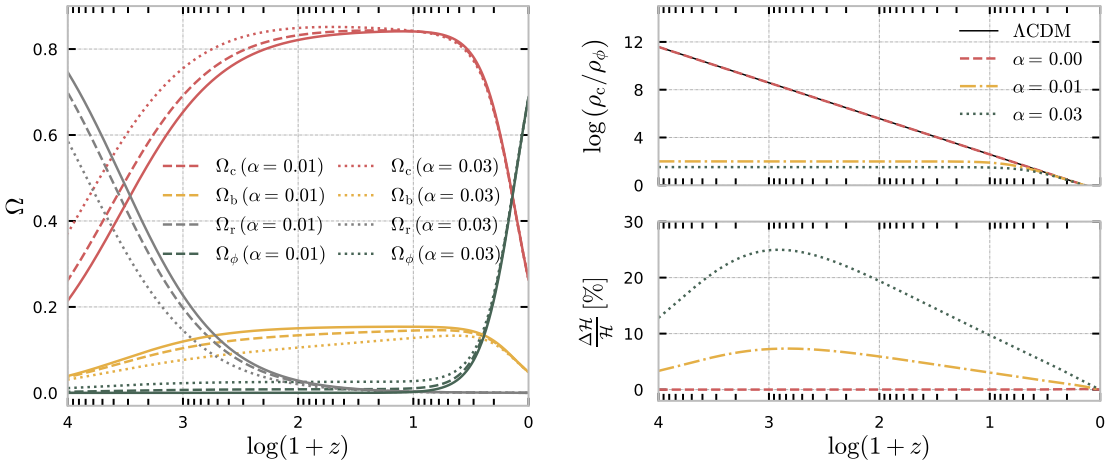

Figure 1: *Left panel*: Evolution of the relative energy densities Ω_i with redshift, $1 + z$, of the scalar field (green), dark matter (red), baryons (yellow) and radiation (grey) for ΛCDM (solid black), $\alpha = 0.01$ (dashed lines) and $\alpha = 0.03$ (dotted lines). *Upper right panel*: Ratio of the energy densities of cold dark matter and dark energy for ΛCDM (solid line), the uncoupled case $\alpha = 0$ (red dashed), $\alpha = 0.01$ (yellow dashed-dotted) and $\alpha = 0.03$ (green dotted). *Lower right panel*: Fractional deviation of the conformal Hubble rate of expansion for the same examples.

compensates for this effect compared to the uncoupled case. This behaviour is illustrated in the left panel of Fig. 1. Consequently, we also see in the figure that the matter-radiation equality occurs at earlier times as the value of α increases. Furthermore, the ϕ field starts acquiring energy at a rate proportional to its energy density and the equality between matter and dark energy occurs earlier. In the lower right panel of Fig. 1 we depict deviations in the Hubble rate for the Kinetic model and the uncoupled case ($\alpha = 0$) compared to ΛCDM. We remark that no significant deviations in $\mathcal{H}$ are observed during the radiation-dominated epoch, as interactions between the dark and radiation sectors are excluded. However, as the matter contribution becomes significant, around $z \approx 10^6$, the Kinetic models exhibit an increased value of $\mathcal{H}$, with this effect becoming more pronounced for higher values of α.

3.2 Evolution of Linear Perturbations

In the Newtonian gauge, we describe the perturbed FLRW metric according to the standard line element [25]:

$$\mathrm{d}s^2 = a^2(\tau)\left[-(1+2\Psi)\,\mathrm{d}\tau^2 + (1-2\Phi)\,\delta_{ij}\mathrm{d}x^i\mathrm{d}x^j\right], \tag{12}$$

where $\Psi(\boldsymbol{x},\tau)$ and $\Phi(\boldsymbol{x},\tau)$ are the Newtonian potentials. Linear perturbations around the gravitational and the background fluid variables are denoted by a δ. The linearised Einstein equations describe the evolution of perturbations for different scales in terms of independent Fourier modes and extra contributions from the dark sector coupling.

The equations that govern the evolution of perturbations in each fluid can be obtained by considering conservation relations and remain as standard for baryons and radiation, which are

non-interacting species. For the coupled DM these become

$$\delta_c' + \theta_c - 3\Phi' = \frac{Q}{\rho_c}\left(\phi'\delta_c - \delta\phi'\right) - \frac{\phi'}{\rho_c}\delta Q\,, \tag{13}$$

$$\theta_c' + \mathcal{H}\theta_c - k^2\Psi = \frac{Q}{\rho_c}\left(\phi'\theta_c - k^2\delta\phi\right)\,, \tag{14}$$

describing the evolution of the density contrast, denoted as $\delta_i = \delta\rho_i/\rho_i$ and the velocity divergence $\theta_i = \nabla \cdot v^{(i)}$. The perturbed coupling term is defined as

$$\begin{aligned}\delta Q = \frac{2\alpha\rho_c}{2\alpha a^2\rho_c + (1+2\alpha)\phi'^2}\Big\{&-3\Phi'\phi' - \phi'\theta_c + \left[3\mathcal{H}\phi' + a^2(V_{,\phi} - Q)\right]\delta_c + \left(2k^2 + a^2V_{,\phi\phi}\right)\delta\phi \\ &- \left[3\mathcal{H}\phi' + 2a^2(V_{,\phi} - Q)\right]\frac{\delta\phi'}{\phi'} + 2a^2\Psi\left(Q - V_{,\phi}\right)\Big\}\,,\end{aligned} \tag{15}$$

and we remark the explicit dependence of δQ on the velocity potential θ_c, which is unusual compared to other coupled dark energy models [18, 26]. Finally, linearisation of the Klein Gordon equation gives:

$$\delta\phi'' + 2\mathcal{H}\delta\phi' + \left(a^2V_{,\phi\phi} + k^2\right)\delta\phi - \left(\Psi' + 3\Phi'\right)\phi' + 2a^2\Psi V_{,\phi} = a^2\delta Q + 2a^2Q\Psi\,. \tag{16}$$

The inclusion of the coupling leaves an imprint on important cosmological observables that can be probed against different data, in particular the matter power spectrum and the temperature-temperature (TT) and lensing angular power spectra of the cosmic microwave background (CMB). Again, assuming standard *Planck* 2018 values for the shape of the scalar primordial power spectrum [12] as well, it is possible to single out the model-specific signatures by taking different sets of $\{\lambda, \alpha\}$ relevant for the scales under consideration.

In the left panel of Fig. 2, we present the linear matter power spectrum at the present time up to the scale $k_{\rm max} = 0.1h$ Mpc^{-1} along with the fractional differences for the Kinetic model in contrast with ΛCDM. We identify an overall suppression at intermediate scales ($10^{-3}h$ Mpc$^{-1} \lesssim k \lesssim 3\times10^{-2}h$ Mpc^{-1}), followed by an enhancement at smaller scales. This effect is primarily related with the global deviation of the turnover in the matter power spectrum to higher k values due to the shift of the radiation-matter equality era to earlier times as identified in the study of the background evolution. The positive exchange of energy from cold dark matter to dark energy at late times inevitably leads to a suppression of the growth of matter perturbations at intermediate scales and an enhancement at smaller scales and the highest deviations are observed for larger values of α. Consequently, the amplitude of the matter power spectrum at the present time and a scale of 8 h^{-1}Mpc, denoted as by σ_8, is expected to be larger for the Kinetic model.

The inclusion of the coupling is also reflected in the evolution of the gravitational potentials, parametrised in terms of the lensing potential $\phi_{\rm lens} = (\Psi + \Phi)/2$ for particular scales. We identify an overall suppression in $\phi_{\rm lens}$ which in turn leads to a suppression of the lensing power spectrum as well, as demonstrated in the right panel of Fig. 2, with this effect becoming more pronounced for larger values of α. On the other hand, the time variation of $\phi_{\rm lens}$ is directly related to the integrated Sachs-Wolfe effect (ISW), imprinted in the shape of the temperature-temperature (TT) power spectrum as a contribution to the radiation transfer function, and is illustrated in the left panel of Fig. 3 as a function of the angular multipole ℓ. This effect comprises two contributions:

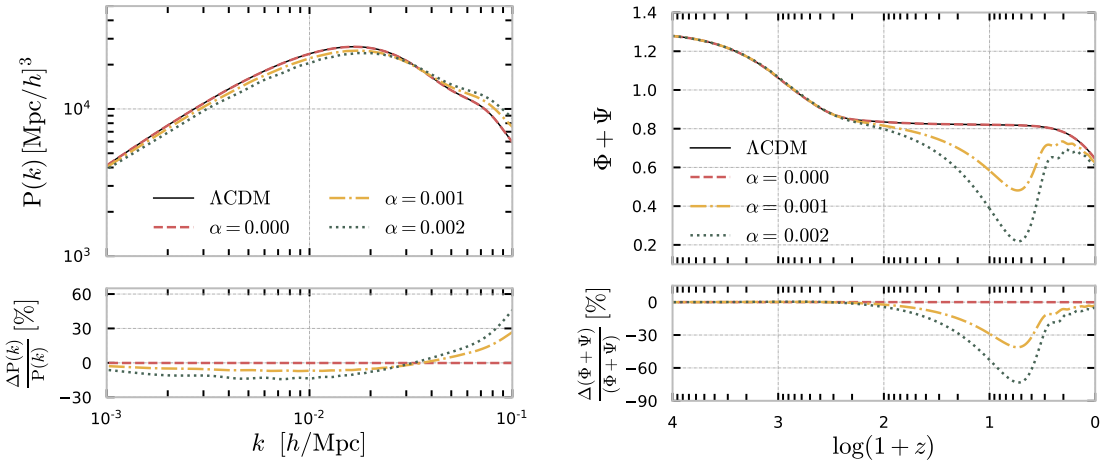

Figure 2: *Left panel*: The matter power spectrum as function of k, for the uncoupled case (dashed red line), $\alpha = 0.001$ (yellow dot-dashed line), $\alpha = 0.002$ (green dotted line) and ΛCDM (black solid line), along with the percentage deviations from the ΛCDM case (lower pannel). *Right panel*: Evolution of the sum of the gravitational potentials as a function of the redshift at $k = 0.01$ Mpc^{-1} for the same examples.

an early-time term occurring during the transition from the radiation- to matter-dominated epochs, shifted to earlier times in the Kinetic model, and a late-time term associated with the dynamics of the dark energy component. We observe a clear overall enhancement compared to the reference case for $\ell \lesssim 300$, with milder differences around the plateau at $\ell < 10$ and the most significant deviations around $\ell \sim 50$. Furthermore, there is a clear increase in the amplitude of the first peak accompanied by a broadening of its shape along with slight variations between the peaks and troughs at higher multipoles. The validity of these combined deviations can be assessed with cosmological data from background observations and the large-scale structure.

4. Observational Constraints

4.1 Data Sets

The baseline data set considered is the CMB *Planck* 2018 [12] data for large angular scales $\ell = [2, 29]$, and a combination of TT, TE, and EE likelihoods for small angular scales $\ell = [30, 2508]$ for TT, and $\ell = [30, 1996]$ for TE cross-correlation and and EE power spectra, referred to as "Plk18" henceforth. We then explore the impact of adding distance and expansion rate measurements, namely baryonic acoustic oscillations (BAO) data from the Sloan Digital Sky Survey (SDSS) DR7 Main Galaxy Sample [27], SDSS DR12 consensus release [28] and the 6dF Galaxy Survey [29], in combination with distance *moduli* measurements of type Ia Supernova (SN) data from Pantheon [30]. This expanded data set is referred to as "Plk18+BAO+SN". Finally, we included CMB lensing potential data from *Planck* 2018 [31, 32] resulting in the data set "Plk18+BAO+SN+len". We use a set of free sampling parameters consisting of the baseline ΛCDM cosmological parameters $(\Omega_b h^2, \Omega_c h^2, z_{reio}, \theta_s, A_s, n_s)$, as well as the two free parameters associated with the Kinetic model (α, λ). We consider flat priors for all the parameters and provide the specific range of values in

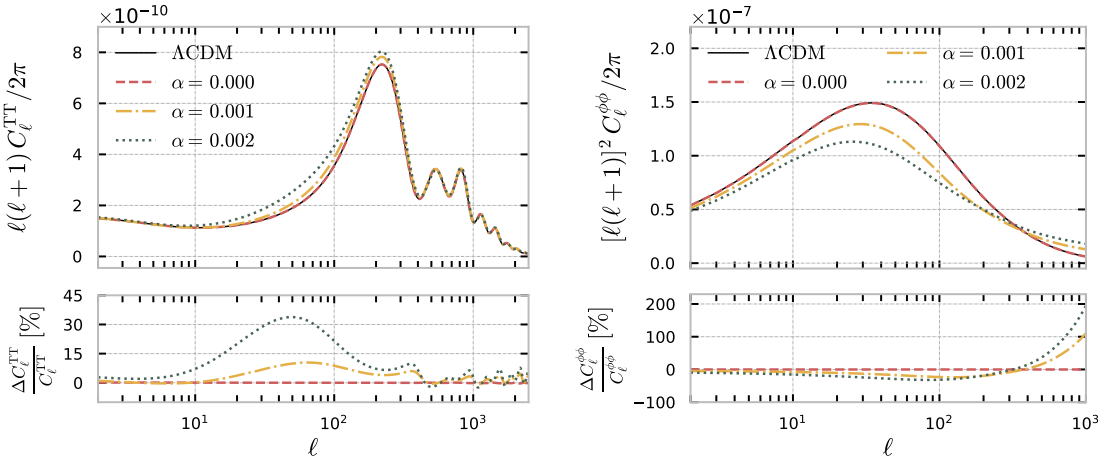

Figure 3: *Left panel*: TT power spectrum of anisotropies as function of the angular scale ℓ, for the uncoupled case (dashed red line), $\alpha = 0.001$ (yellow dot-dashed line), $\alpha = 0.002$ (green dotted line) and ΛCDM (black solid line) for reference, along with percentage deviations with respect to ΛCDM (lower panel). *Right panel*: Lensing angular power spectra for the same examples and relative difference between the predictions for each model and for ΛCDM.

Table I of Ref. [15]. Our analysis also yields derived constraints on H_0 and $S_8^0 = \sigma_8^0\sqrt{\Omega_m^0/0.3}$. The latter is also known to be in tension with cosmic shear measurements [7, 8, 33] for the standard model, with CMB data favouring higher values. Finally, to produce the Monte Carlo Markov Chain (MCMC) samples we resort to our personal modification of the Einstein Boltzmann solver `CLASS` [22–24] interfaced with the `Monte Python` sampler [34, 35], following the Metropolis-Hastings algorithm. Subsequently, we analyse the MCMC chains and produce the results reported in Ref. [15], resorting to the `GetDist` Python package [36].

4.2 Results

In Tables 1 and 2 we present the constraints on the sampled parameters for the Kinetic and ΛCDM models, respectively. These results are illustrated in Fig. 4 where the corresponding 2D contour plots for all the considered combinations of data sets are displayed. Although the constraints on the cosmological parameters of the Kinetic model are compatible with those of the ΛCDM case within the uncertainties, the latter yields higher mean values for H_0 and Ω_m^0. The Kinetic model exhibits a positive correlation between H_0 and Ω_m^0, opposite to the anti-correlation observed in the ΛCDM model. This characteristic correlation persists across all the three data combinations considered and is ascribed to the non-zero prediction for the α parameter, which enhances the TT power spectrum. Furthermore, Fig. 4 depicts contour plots for the constraints in the $S_8^0 - \Omega_m^0$ plane. Both the standard and extended models exhibit a positive correlation between these parameters. With only the Plk18 data, we find $S_8^0 = 0.793^{+0.110}_{-0.064}$ at a 68% confidence level (C.L.) in the Kinetic model, thereby mitigating the discordance with cosmic shear measurements in the standard model ($S_8^0 = 0.833 \pm 0.016$). However, when considering other data sets, the discrepancy reemerges, indicating tensions between the BAO and/or SN data within this framework. A similar situation has

Kinetic Model			
Parameter	Plk18	Plk18+BAO+SN	Plk18+BAO+SN+len
S_8^0	$0.793^{+0.110}_{-0.064}$	$0.875^{+0.037}_{-0.043}$	$0.863^{+0.030}_{-0.039}$
Ω_m^0	$0.257^{+0.045}_{-0.025}$	$0.2988^{+0.0072}_{-0.0036}$	$0.2982^{+0.0070}_{-0.0035}$
H_0	$64.0^{+3.3}_{-1.8}$	67.14 ± 0.62	$66.94^{+0.60}_{-0.54}$
$10^{-9}A_s$	2.088 ± 0.035	2.096 ± 0.035	2.111 ± 0.031
n_s	0.9667 ± 0.0047	0.9669 ± 0.0044	0.9655 ± 0.0041
λ	1.11 ± 0.48	$0.42^{+0.18}_{-0.21}$	$0.41^{+0.17}_{-0.22}$
$10^4\alpha$	1.88 ± 0.95	$1.37^{+0.67}_{-1.00}$	$1.05^{+0.51}_{-0.87}$

Table 1: 68% C.L. bounds on the cosmological and model parameters for the Kinetic model for the three different combinations of data sets: *Planck*, *Planck* combined with BAO and SN, and their full combination with CMB lensing.

been observed in a Galileon model [37], suggesting a potential bias towards ΛCDM-like models in the BAO data [38].

The results for the specific parameters of the Kinetic model can be appreciated in the 2D contour plots of Fig. 5, where we see that the coupling parameter α is consistently constrained to be of the order 10^{-4}, regardless of the data set combination. When considering only the Planck data, a higher mean value of α is preferred, primarily to better accommodate the TT likelihood. However, incorporating BAO and SN data slightly reduces the mean value of α. Furthermore, adding CMB lensing data shifts the peak of the posterior distribution for α to an even lower central value. This behaviour is associated with the reported lensing excess by the Planck collaboration [12, 39]. In the Kinetic model, the lensing power spectrum is always suppressed compared to the ΛCDM scenario, with higher values of α corresponding to lower amplitudes. Consequently, a lower mean value of α is favoured to better match the CMB lensing data.

The inclusion of BAO and SN data leads to narrower constraints on Ω_m^0, resulting in tighter constraints on other parameters such as H_0, S_8^0, and λ. The parameter λ is directly connected to the anti-correlation displayed in Fig. 5 in the $\Omega_m^0 - \lambda$ plane, where higher values of Ω_m^0 correspond to lower values of λ. This negative correlation arises from considering that the late-time accelerated expansion is primarily regulated by two parameters: Ω_ϕ and λ. The Friedmann constraint for flatness gives $\Omega_\phi \approx 1 - \Omega_m^0$ at late times, implying that higher values of Ω_m^0 are associated with lower values of Ω_ϕ^0. Consequently, to achieve a cosmological constant-like scenario for the scalar field at present times, the mean value of λ is pushed towards smaller values, explaining the identified anti-correlation between Ω_m^0 and λ.

5. Model Selection analysis

Lastly, we aim to evaluate whether the Kinetic model is favoured over the ΛCDM case resorting to different statistical indicators for comparison purposes. First, we simply evaluate the effective χ^2-statistics, corresponding to the maximum likelihood, denoted as $\chi^2_{\rm eff}$, and which allows us to determine how well the Kinetic model fits the data when compared to ΛCDM. This is accomplished by calculating $\Delta\chi^2_{\rm eff} = \chi^2_{\rm eff,Kinetic} - \chi^2_{\rm eff,\Lambda CDM}$, where a negative value indicates support for the

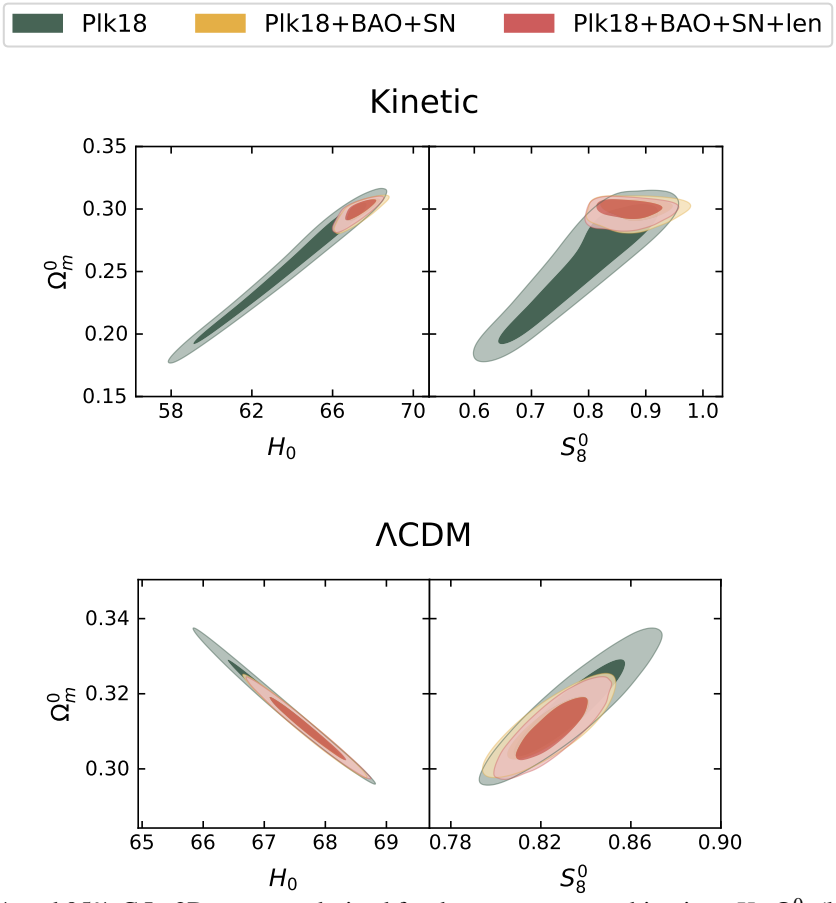

Figure 4: 68% and 95% C.L. 2D contours derived for the parameter combinations H_0-Ω_m^0 (left panels) and S_8^0-Ω_m^0 (right panels) in the Kinetic model (upper panels) and ΛCDM model (lower panels) for the *Planck* 2018 data (green), the *Planck* 2018, BAO and SN combination (yellow), and their combination with CMB lensing(red).

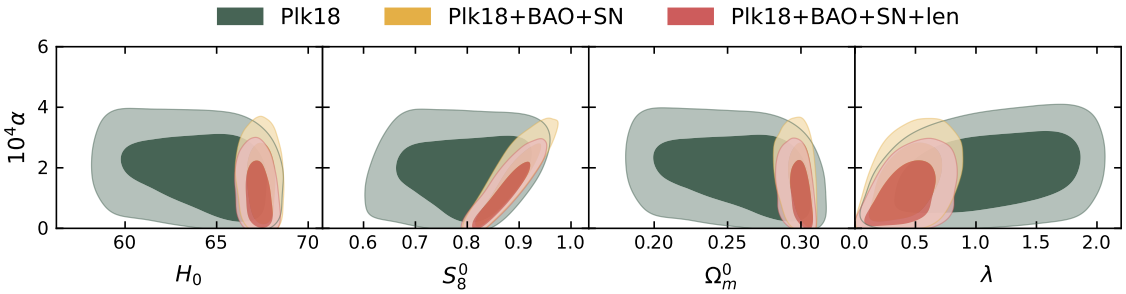

Figure 5: 68% and 95% C.L. contours obtained in the Kinetic model for the *Planck* 2018 data (green), the *Planck* 2018, BAO and SN combination (yellow), and their combination with CMB lensing (red).

Kinetic model, while a positive value suggests otherwise. On the other hand, in order to statistically compare the level of support for one model against the other, we calculate the Bayes factor of an extended model relative to ΛCDM. The Bayes factor of an extended model i with respect to the

ΛCDM Model			
Parameter	Plk18	Plk18+BAO+SN	Plk18+BAO+SN+len
S_8^0	0.833 ± 0.016	$0.831^{+0.013}_{-0.015}$	0.834 ± 0.013
Ω_m^0	0.3163 ± 0.0085	$0.3151^{+0.0060}_{-0.0075}$	0.3162 ± 0.0073
H_0	67.31 ± 0.61	$67.39^{+0.53}_{-0.45}$	67.32 ± 0.53
$10^{-9}A_s$	2.102 ± 0.034	2.102 ± 0.034	$2.105^{+0.028}_{-0.032}$
n_s	0.9652 ± 0.0044	0.9656 ± 0.0039	0.9651 ± 0.0041

Table 2: 68% C.L. bounds on the cosmological parameters for the ΛCDM model for the three different combinations of data sets: *Planck* 2018, *Planck* 2018 combined with BAO and SN, and and their full combination with CMB lensing.

ΛCDM model is given by [REF]

$$B_{K,\Lambda\mathrm{CDM}} = \frac{P(\mathcal{D}|K)}{P(\mathcal{D}|\Lambda\mathrm{CDM})}, \tag{17}$$

which we calculated employing the `MCEvidence` code [40] and where $\mathcal{D}$ represents a given data set and $P(\mathcal{D}|K)$ and $P(\mathcal{D}|\Lambda\mathrm{CDM})$ are the evidences for the Kinetic and ΛCDM models, respectively. We see that the greater the evidence for the Kinetic model relative to ΛCDM, the larger the Bayes factor $B_{K,\Lambda\mathrm{CDM}}$ will be. The numerical Bayes factor may be translated into a qualitative statement about the strength of evidence for an extended model against ΛCDM through the use of Jeffrey's scale [41]. According to this criteria the conclusive range of values of $\ln B_{K,\Lambda\mathrm{CDM}}$ imply weak ($[1, 2.5]$), moderate ($[2.5, 5]$) or strong evidence (> 5). If the value is negative then there is no evidence of support for the Kinetic model over ΛCDM and if $|\ln B_{K,\Lambda\mathrm{CDM}}| < 1$ then nothing can be concluded using the data set $\mathcal{D}$.

In Tab. 3 we present the values for both the $\Delta\chi^2_{\mathrm{eff}}$ and the $\ln B_{K,\Lambda\mathrm{CDM}}$, along with the corresponding individual values. From the analysis, we find that when considering only the Plk18 data, the Kinetic model shows a slightly better fit to the data compared to the ΛCDM model, with a decrease in the chi-squared value of $\Delta\chi^2 = -0.9$. However, this preference disappears when other data sets are included. This is mainly due to the BAO and SN data affecting the fit to the temperature-temperature (TT) likelihood, which worsens after incorporating the CMB lensing data.

Data Sets $\mathcal{D}$ / Statistics	Plk18	Plk18+BAO+SN	Plk18+BAO+SN+len
ΛCDM χ^2_{eff}	2771.1	3804.62	3813.92
$\ln B_{\Lambda\mathrm{CDM}}$	−1423.2	−1941.0	−1945.1
Kinetic χ^2_{eff}	2770.2	3805.32	3814.92
$\ln B_K$	−1427.4	−1946.3	−1951.8
$\Delta\chi^2_{\mathrm{eff}}$	−0.9	0.7	1.0
$\ln B_{K,\Lambda\mathrm{CDM}}$	−4.2	−5.4	−6.8

Table 3: Results for the $\Delta\chi^2_{\mathrm{eff}}$ and the Bayesian evidence ratio $\ln B_{K,\Lambda\mathrm{CDM}}$ obtained for the Kinetic and ΛCDM scenarios.

The Kinetic model predicts a suppressed lensing amplitude, whereas the CMB lensing data actually indicates an excess of power. However, any support for the Kinetic model becomes insignificant when considering the Bayesian evidence, for which we report negative values across all the data sets. This is directly related with the increased complexity of the Kinetic model, with the inclusion of two additional parameters resulting in either reduced or no improvement at all in the fitting to the data. Therefore, we can conclude that there is no statistical evidence for the Kinetic model in this analysis.

6. Discussion

In this study, we investigated a Kinetic model consisting of a coupled quintessence theory with a power-law kinetic interaction, and explored its impact on the evolution of the background and linear perturbations in the Universe. We analysed the relevant cosmological observables and derived constraints on the model parameters using various data sets, including CMB, CMB lensing, BAO, and SN data.

We first performed a numerical study of the predictions of the model to assess the valid parameter space with physical interest, resorting to a modified version of the publicly available Einstein-Boltzmann code `CLASS`. At the background level, we found that a non-zero value of α allows for a scaling regime during the radiation-dominated epoch, where the ratio of the densities of cold dark matter and the scalar field approximately scale with α. We identified that only energy transfer from DM to DE can be realised in such scenarios. Additionally, the radiation-matter equality is shifted towards earlier times, with direct consequences on the matter power spectrum, namely a suppression of small-scale power and an enhancement of large-scale growth compared to the ΛCDM model. Consequently, we observed an overall suppression of the lensing potential and modifications in the ISW effect, which alter the shape of the temperature power spectrum of anisotropies at large angular scales.

Using an MCMC method for cosmological parameter extraction, we applied the theoretical insight gained in the numerical study to constrain the model. We found that the tension in S_8^0 was apparently alleviated, with $S_8^0 = 0.793^{+0.110}_{-0.064}$ at 68% confidence level using *Planck* data only, while the tension in H_0 persisted. Regardless of the combination of data sets considered, the parameter α was consistently constrained to be on the order of 10^{-4}. We also reported constraints on the other parameter of the Kinetic model, λ, with the strongest bounds being obtained when combining BAO and SN data. This is primarily caused by the strong constraining power of BAO data on Ω_m^0, which indirectly affects the bounds on λ. Finally, we presented a model selection study using the effective $\chi^2_{\rm eff}$ and the Bayesian evidence, with the latter indicating statistical preference for ΛCDM over the Kinetic toy-model related to the increased dimension of the parameter space. In conclusion, we highlight the importance of considering the Kinetic model and other variations for future investigations, especially with the availability of new probes from upcoming surveys. Further studies using high-precision data will help resolve tensions and establish a definitive preference for one model over the other, possibly hinting at more complicated shapes for the kinetic function.

Acknowledgments

E.M.T. is supported by the grant SFRH/BD/143231/2019 from Fundação para a Ciência e a Tecnologia (FCT). E.M.T. also acknowledges the FCT project with Ref. number PTDC/FIS-AST/0054/2021 and the COST Action CA21136 Addressing observational tensions in cosmology with systematics and fundamental physics (CosmoVerse) supported by COST (European Cooperation in Science and Technology). The results of this work were possible thanks to The University of Sheffield's High Performance Computing (HPC) clusters Bessemer and ShARC. Lastly, E.M.T. thanks the organisers and participants of the "Tensions in Cosmology" session of the Corfu Summer Institute 2022 for the enjoyable and fruitful workshop.

References

[1] S.M. Carroll, *The cosmological constant*, *Living Reviews in Relativity* **4** (2001) .

[2] Supernova Search Team collaboration, *Observational evidence from supernovae for an accelerating universe and a cosmological constant*, *Astron. J.* **116** (1998) 1009 [astro-ph/9805201].

[3] Supernova Cosmology Project collaboration, *Measurements of Omega and Lambda from 42 high redshift supernovae*, *Astrophys. J.* **517** (1999) 565 [astro-ph/9812133].

[4] S. Weinberg, *The Cosmological Constant Problem*, *Rev. Mod. Phys.* **61** (1989) 1.

[5] S. Weinberg, *The Cosmological constant problems*, astro-ph/0005265.

[6] J. Martin, *Everything You Always Wanted To Know About The Cosmological Constant Problem (But Were Afraid To Ask)*, *Comptes Rendus Physique* **13** (2012) 566 [1205.3365].

[7] E. Di Valentino et al., *Cosmology intertwined III: $f\sigma_8$ and S_8*, *Astropart. Phys.* **131** (2021) 102604 [2008.11285].

[8] E. Abdalla et al., *Cosmology intertwined: A review of the particle physics, astrophysics, and cosmology associated with the cosmological tensions and anomalies*, *JHEAp* **34** (2022) 49 [2203.06142].

[9] A.G. Riess, S. Casertano, W. Yuan, L.M. Macri and D. Scolnic, *Large Magellanic Cloud Cepheid Standards Provide a 1% Foundation for the Determination of the Hubble Constant and Stronger Evidence for Physics beyond ΛCDM*, *Astrophys. J.* **876** (2019) 85 [1903.07603].

[10] K.C. Wong et al., *H0LiCOW – XIII. A 2.4 per cent measurement of H0 from lensed quasars: 5.3σ tension between early- and late-Universe probes*, *Mon. Not. Roy. Astron. Soc.* **498** (2020) 1420 [1907.04869].

[11] D.W. Pesce et al., *The Megamaser Cosmology Project. XIII. Combined Hubble constant constraints*, *Astrophys. J. Lett.* **891** (2020) L1 [2001.09213].

[12] Planck collaboration, *Planck 2018 results. VI. Cosmological parameters*, *Astron. Astrophys.* **641** (2020) A6 [1807.06209].

[13] A.G. Riess et al., *A Comprehensive Measurement of the Local Value of the Hubble Constant with 1 km s^{-1} Mpc^{-1} Uncertainty from the Hubble Space Telescope and the SH0ES Team*, *Astrophys. J. Lett.* **934** (2022) L7 [2112.04510].

[14] CANTATA collaboration, *Modified Gravity and Cosmology: An Update by the CANTATA Network*, 2105.12582.

[15] E.M. Teixeira, B.J. Barros, V.M.C. Ferreira and N. Frusciante, *Dissecting kinetically coupled quintessence: phenomenology and observational tests*, *JCAP* **11** (2022) 059 [2207.13682].

[16] B.J. Barros, *Kinetically coupled dark energy*, *Phys. Rev. D* **99** (2019) 064051 [1901.03972].

[17] V. Pettorino, *Testing modified gravity with Planck: the case of coupled dark energy*, *Phys. Rev. D* **88** (2013) 063519 [1305.7457].

[18] C. van de Bruck, J. Mifsud and J. Morrice, *Testing coupled dark energy models with their cosmological background evolution*, *Phys. Rev. D* **95** (2017) 043513 [1609.09855].

[19] B.J. Barros, L. Amendola, T. Barreiro and N.J. Nunes, *Coupled quintessence with a ΛCDM background: removing the σ_8 tension*, *JCAP* **01** (2019) 007 [1802.09216].

[20] A. Gómez-Valent, V. Pettorino and L. Amendola, *Update on coupled dark energy and the H_0 tension*, *Phys. Rev. D* **101** (2020) 123513 [2004.00610].

[21] R. Bean, E.E. Flanagan, I. Laszlo and M. Trodden, *Constraining Interactions in Cosmology's Dark Sector*, *Phys. Rev. D* **78** (2008) 123514 [0808.1105].

[22] J. Lesgourgues, *The cosmic linear anisotropy solving system (class) i: Overview*, 2011.

[23] D. Blas, J. Lesgourgues and T. Tram, *The cosmic linear anisotropy solving system (class). part ii: Approximation schemes*, *Journal of Cosmology and Astroparticle Physics* **2011** (2011) 034–034.

[24] J. Lesgourgues, *The cosmic linear anisotropy solving system (class) iii: Comparision with camb for lambdacdm*, 2011.

[25] C.-P. Ma and E. Bertschinger, *Cosmological perturbation theory in the synchronous and conformal Newtonian gauges*, *Astrophys. J.* **455** (1995) 7 [astro-ph/9506072].

[26] C. van de Bruck and E.M. Teixeira, *Dark D-Brane Cosmology: from background evolution to cosmological perturbations*, 2007.15414.

[27] A.J. Ross, L. Samushia, C. Howlett, W.J. Percival, A. Burden and M. Manera, *The clustering of the SDSS DR7 main Galaxy sample – I. A 4 per cent distance measure at $z = 0.15$*, *Mon. Not. Roy. Astron. Soc.* **449** (2015) 835 [1409.3242].

[28] BOSS collaboration, *The clustering of galaxies in the completed SDSS-III Baryon Oscillation Spectroscopic Survey: baryon acoustic oscillations in the Fourier space*, *Mon. Not. Roy. Astron. Soc.* **464** (2017) 3409 [1607.03149].

[29] F. Beutler, C. Blake, M. Colless, D.H. Jones, L. Staveley-Smith, L. Campbell et al., *The 6dF Galaxy Survey: Baryon Acoustic Oscillations and the Local Hubble Constant*, *Mon. Not. Roy. Astron. Soc.* **416** (2011) 3017 [1106.3366].

[30] Pan-STARRS1 collaboration, *The Complete Light-curve Sample of Spectroscopically Confirmed SNe Ia from Pan-STARRS1 and Cosmological Constraints from the Combined Pantheon Sample*, *Astrophys. J.* **859** (2018) 101 [1710.00845].

[31] Planck collaboration, *Planck 2018 results. V. CMB power spectra and likelihoods*, *Astron. Astrophys.* **641** (2020) A5 [1907.12875].

[32] Planck collaboration, *Planck 2018 results. VIII. Gravitational lensing*, *Astron. Astrophys.* **641** (2020) A8 [1807.06210].

[33] C. Heymans et al., *KiDS-1000 Cosmology: Multi-probe weak gravitational lensing and spectroscopic galaxy clustering constraints*, *Astron. Astrophys.* **646** (2021) A140 [2007.15632].

[34] B. Audren, J. Lesgourgues, K. Benabed and S. Prunet, *Conservative constraints on early cosmology with montepython*, *Journal of Cosmology and Astroparticle Physics* **2013** (2013) 001.

[35] T. Brinckmann and J. Lesgourgues, *MontePython 3: boosted MCMC sampler and other features*, 1804.07261.

[36] A. Lewis, *GetDist: a Python package for analysing Monte Carlo samples*, 1910.13970.

[37] N. Frusciante, S. Peirone, L. Atayde and A. De Felice, *Phenomenology of the generalized cubic covariant Galileon model and cosmological bounds*, *Phys. Rev. D* **101** (2020) 064001 [1912.07586].

[38] P. Carter, F. Beutler, W.J. Percival, J. DeRose, R.H. Wechsler and C. Zhao, *The impact of the fiducial cosmology assumption on BAO distance scale measurements*, *Mon. Not. Roy. Astron. Soc.* **494** (2020) 2076 [1906.03035].

[39] Planck collaboration, *Planck 2015 results. I. Overview of products and scientific results*, *Astron. Astrophys.* **594** (2016) A1 [1502.01582].

[40] A. Heavens, Y. Fantaye, A. Mootoovaloo, H. Eggers, Z. Hosenie, S. Kroon et al., *Marginal Likelihoods from Monte Carlo Markov Chains*, 1704.03472.

[41] R.E. Kass and A.E. Raftery, *Bayes Factors*, *J. Am. Statist. Assoc.* **90** (1995) 773.